Wavelength Doubling Cascade to Möbius Defect Turbulence in a 3D Anisotropic Liquid

Cécile Fradin,[1,2] P. L. Finn,[1] Helmut R. Brand,[3,1] and P. E. Cladis[1,3,4]
[1]*Bell Laboratories, Lucent Technologies, Murray Hill, New Jersey 07974*
[2]*Service de Physique de l'État Condensé, CEA Saclay, F 91191 Gif-sur-Yvette Cedex, France*
[3]*Theoretische Physik III, Universität Bayreuth, D-95440 Bayreuth, Germany*
[4]*Advanced Liquid Crystal Technologies, P.O. 1314, Summit, New Jersey 07902*
(Received 26 June 1998)

The following wavelength doubling cascade from a uniform state to a turbulent pattern is observed in a 3D anisotropic liquid: First oscillating convective rolls followed by a stationary stripe pattern, then Möbius defect creation stabilizing an unusual curved roll pattern that eventually becomes turbulent. Once created, Möbius defects are topologically trapped and the initial uniform state is not recovered. The system experimentally investigated is electroconvection above a highly nonlinear base state. [S0031-9007(98)07240-8]

PACS numbers: 47.54.+r, 05.70.Ln, 47.27.–i, 61.30.Gd

One of the many reasons for the growing interest [1–3] in patterns formed and the onset of turbulence in 3D anisotropic liquids is that they reveal by controlled experiments the intricate interplay between spatial and temporal order. In particular, in the 3D anisotropic liquids, liquid crystals [4], and superfluid ^{3}He [5], the interplay between flow fields and the orientational ordering field generates qualitative and quantitative information relevant to deep insights in natural laws derived from nonlinear field theories [6].

The subharmonic (wavelength doubling) cascade, described here for the first time (Fig. 1) and not predicted by any theory, shows a new route to spatiotemporal disorder in an orientationally ordered liquid. The orientational order has complete rotational freedom in planes perpendicular to the driving force. Two remarkable consequences of this freedom are traveling rolls built on a highly nonlinear base state and orientational order that consistently evades containment in vortex flow shear planes $\perp$ to the roll axes, **R**. A line of roll disclinations with the same topological charge spontaneously forms to finally lock the orientational order $\perp \mathbf{R}$. The result is an unusual curved roll pattern that we call the Zvinger pattern, in analogy to a cage for wild animals, as the orientational order rotates 2π in a Zvinger wavelength, λ_Z. When the external driving force is removed from Zvingers, a state with a length scale emerges that coarsens extremely slowly to the uniform state by defect motion (Fig. 2).

This novel cascade is observed in a nematic liquid crystal [7]. In many organic materials, a nematic phase intervenes between the isotropic liquid and other more ordered thermodynamic phases. It is characterized by long range orientational order in a preferred direction, $\hat{\mathbf{n}}$. As $\hat{\mathbf{n}}$ is not polar, its only line defect is a $\pm\pi$ rotation of $\hat{\mathbf{n}}$ around a singular line. As a $\pm\pi$ rotation is used to create the "endless" surface of a Möbius band, Frank has called them Möbius disclinations [8].

Möbius disclinations, *Möbions*, have a topological charge $S = \pm 1/2$ because in a circuit around the defect line, $\mathbf{n}$ rotates $\pm\pi = S \times 2\pi$. Viewed along its line between crossed polarizers, $S = \pm 1/2$ disclinations are characterized by two black "brushes" when $\hat{\mathbf{n}}$ is parallel to either the polarizer or the analyzer. For a Möbion, this occurs twice in one circuit (e.g., Fig. 2). Because the elastic energy diverges at the singular line, Möbions are usually not observed. Rather, one observes nonsingular $S = \pm 1$

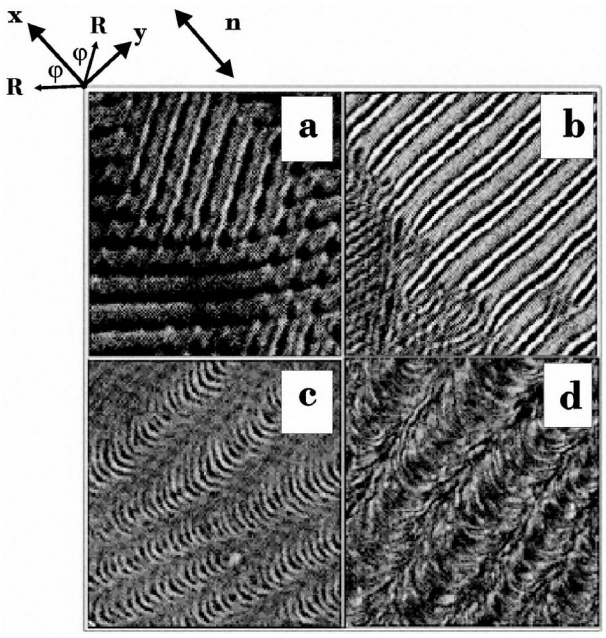

FIG. 1. The wavelength doubling cascade in an xy plane viewed between crossed polarizers. $d = 18\ \mu$m. (a) Traveling degenerate rolls. $\nu = 50$ Hz, $\lambda \sim d$, and the roll axes (**R**) are $\phi = \pm 30°$ to $\hat{\mathbf{n}}$ in the xz plane. (b) Transition from traveling degenerate rolls (bottom left) to the stationary stripe pattern (top right). $\nu = 300$ Hz, $\lambda_S = 2\lambda$. (c) Transition from the stripe pattern (top left) to the Zvinger pattern of curved rolls viewed with one polarizer. $\hat{\mathbf{n}} \perp \hat{\mathbf{R}}$. $\lambda_Z = 4\lambda$. Note Zvinger dislocation even near onset. (d) Fully developed Zvingers viewed between crossed polarizers. The area shown is 112.5 μm $\times$ 105 μm. Total sample area is 1 cm $\times$ 1 cm.

 0031-9007/98/81(14)/2902(4)$15.00

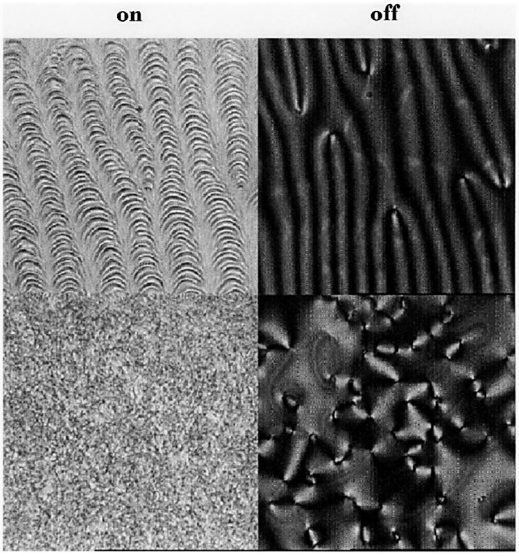

FIG. 2. The Zvinger pattern and Möbion turbulence when the electric field is on (left) and off (right). The Zvinger pattern off-state (top right) shows regular nearly vertical dark lines (brushes) of the uniform rotation of $\hat{\mathbf{n}}$ in the Zvinger pattern. In the Möbion turbulence off-state (bottom right), Möbions are irregularly distributed and larger in number. Magnification as in Fig. 1.

defects, characterized by four black brushes and a finite total energy [9]. From an equilibrium perspective then, a surprising feature of this wavelength doubling cascade (Fig. 1) is that it spontaneously generates Möbions of only one sign: $S = +1/2$. This seems to be because elastic deformations of a single roll lead only to $S = +1/2$ disclinations. As the total topological charge is not zero, $\hat{\mathbf{n}}$ cannot simply relax to a uniform state (Fig. 2).

The instability studied is electroconvection (EC), where an ac electric field, $\mathbf{E}$, is applied to a thin nematic layer (thickness $d = 10{-}20\ \mu$m) [7,10] with a negative dielectric anisotropy, $\varepsilon_a < 0$: in a large enough field, $\hat{\mathbf{n}} \perp \mathbf{E}$. The frequency, ν, of the applied field is such that $\nu < \nu_c$ so that charge motion creating the convective flow field follows $\mathbf{E}$. $\nu_c \sim 450$ Hz is experimentally determined.

The material is prepared so that initially $\hat{\mathbf{n}} \parallel \mathbf{E}$ (Fig. 3a), i.e., homeotropic boundary conditions. As torques exerted on $\hat{\mathbf{n}}$ by $\mathbf{E}$ compete with those from boundary conditions, there is a boundary layer of thickness, $\xi \propto 1/E \sim 0.5{-}2\ \mu$m in these experiments. This fluid boundary layer allows $\hat{\mathbf{n}}$ complete rotational freedom in planes $\perp \mathbf{E}$.

As usual, the instabilities are viewed along $\mathbf{E}$ through transparent electrodes with a polarizing microscope interfaced to a video camera and computer controlled image analysis system. When the applied voltage V is $V > V_F \sim 4.5$ V, the Fréedericksz transition voltage [11], $\hat{\mathbf{n}}$ acquires a component, n_x, in the sample midplane $\perp \mathbf{E}$ ($\theta \gtrsim 0$ in Fig. 3b). While n_x can be anywhere in the xy plane, to minimize its elastic energy with well-prepared homeotropic boundary conditions, an $\hat{\mathbf{x}}$ is quickly selected

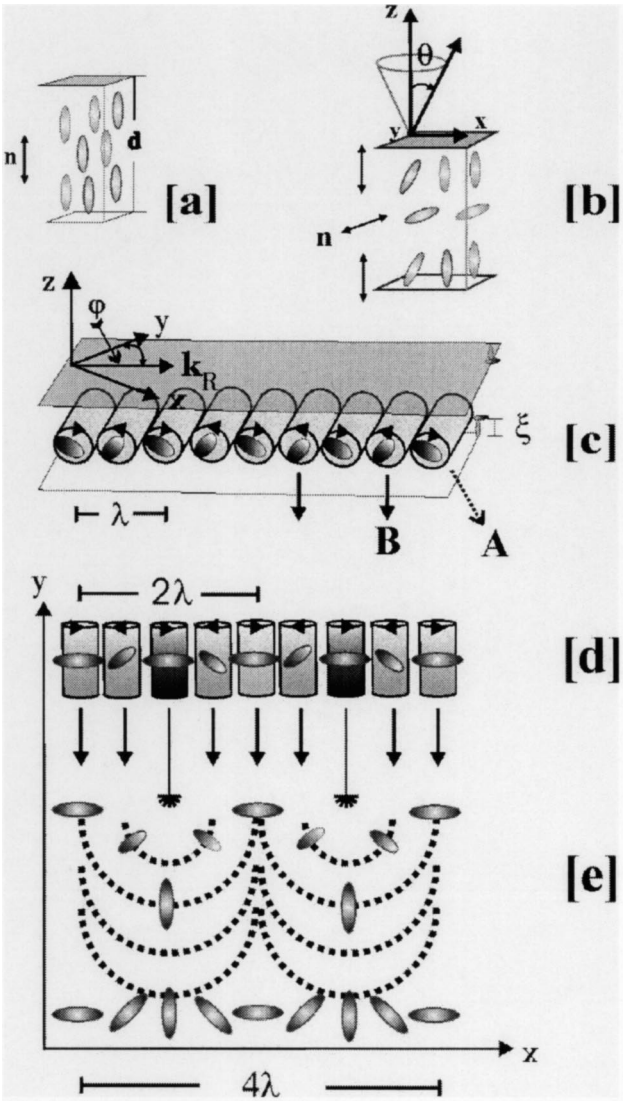

FIG. 3. (a) The initial state: $\hat{\mathbf{n}} \parallel \hat{\mathbf{z}} \parallel \mathbf{E}$. Sample thickness is d. (b) $V > V_F$: $n_x/n_z = \tan\theta$, $n_y = 0$. (c) $V > V_c$: Traveling degenerate tilted rolls, wavelength λ. Viscous torques increase n_x in half the rolls (A) and decrease it in adjacent ones (B). While $n_y = 0$ as in (b), the roll axes, $\mathbf{R}$ (wave vector, $\mathbf{k_R}$), is at an angle $\pm\phi$ to $\hat{\mathbf{n}}$ ($\hat{\mathbf{y}}$). Rolls travel with $\mathbf{v_t} \parallel \mathbf{k_R}$. (d) $V > V_S$: Standing stripe pattern, $\lambda_S = 2\lambda$, small amplitude n_y modulation. Max and min in n_y are associated with B rolls [vertical arrows in (c)]. $n_y \neq 0$ sets up torques creating only $S = +1/2$ disclinations in $\mathbf{R}$ tracked by arrows between (d) and (e) with core rolls darker. (e) $V > V_Z$: Zvinger pattern, $\lambda_Z = 2\lambda_S = 4\lambda$. $\mathbf{R}$ shown as dotted. The Zvinger pattern nucleates from roll disclinations at the Zvinger-stripe interface [(d), (e)]. Note roll flow readjustment between core rolls. $\hat{\mathbf{n}}$ has complete xy freedom and $\hat{\mathbf{n}} \perp \mathbf{R}$.

locally so that variations in $\hat{\mathbf{n}}$ are only in an xz plane. With increasing V, $\theta \to \pi/2$. As $\theta > \pi/2$ launches known director instabilities [7], not observed in these experiments, $\theta = \pi/2$ is an upper bound. We stress that the Fréedericksz transition sets up a highly nonlinear state for the curvature elasticity of $\hat{\mathbf{n}}$ well before electroconvection onset at $V_c > 2V_F$.

With no external field selecting a preferred direction for $\hat{\mathbf{n}}$, the recent theoretical prediction is a direct transition from a disordered director configuration to turbulence in EC patterns observed as a function of the two control parameters $\varepsilon = (V^2 - V_c^2)/V_c^2$ and ν [12]. Indeed, in contrast to observations presented here, previously reported patterns at EC onset in the homeotropic geometry are irregular and nonstationary [13,14].

Here, we observe an unexpected wavelength doubling sequence mediating the transition to Möbius defect turbulence. The only difference between the material here, $10E6$ [15–18], and the ones used previously [13,14] is that, in the temperature range of this study, $10E6$'s rotational viscous coefficient, γ_1, is slightly smaller than its extensional one, $|\gamma_2|$ [15]. In materials used in previous experiments [13,14], $\gamma_1 \gtrsim |\gamma_2|$. The qualitative difference between the two cases turns on the question of flow alignment for $\hat{\mathbf{n}}$. When $\gamma_1 \gtrsim |\gamma_2|$, viscous torques in a shear plane containing $\hat{\mathbf{n}}$ are bounded. The consequence is a stationary flow aligned orientation for $\hat{\mathbf{n}}$. In $10E6$, $\gamma_1 \lesssim |\gamma_2|$. In this case, viscous torques are unbounded so $\hat{\mathbf{n}}$ continuously rotates until stopped by elastic torque buildup [7,15].

The wavelength doubling scenario is also not observed in samples where boundary conditions define a preferred direction, $\hat{\mathbf{x}}$, with $\hat{\mathbf{n}} \parallel \hat{\mathbf{x}}$. In this planar geometry, the EC patterns are built on an initially uniform state, $\hat{\mathbf{n}} \perp \hat{E}$. The first instability in $10E6$ for this geometry [15] is consistent with a predicted forward bifurcation [10] to a stationary normal roll pattern ($\mathbf{R} \perp \hat{\mathbf{n}}$). Its wavelength, λ_p, nearly halves as ν increases from $\nu = 10$ Hz to $\nu = 350$ Hz [17].

The first instability built on the initially nonlinear base state (Fig. 1b) differs on several counts from that built on the initially uniform one [15]. First, because of the boundary layer, its wavelength, λ, is smaller: $\lambda \sim \lambda_p/2$, while V_c vs ν is similar: $12 < V_c < 40$ V for $10 < \nu < 350$ Hz. Second, $\mathbf{R}$ is at an angle $\pm\phi$ to $\hat{\mathbf{n}}$ (Figs. 1a, 3c, 4). Third, rolls travel with a speed v_t with $\mathbf{v_t} \perp \mathbf{R}$. As $\pm v_t$ are observed, this is a Hopf bifurcation. Fourth, as $\mathbf{R} \to \mathbf{R} \perp \hat{\mathbf{n}}$ ($\phi \to \pi/2$, $\nu \to 350$ Hz), rolls travel faster.

But, the pattern velocity, $\mathbf{v_p} \perp \hat{\mathbf{n}}$ ($|\mathbf{v_p}| \equiv |\mathbf{v_t}| \cos\phi = 32\ \mu$m/s), is independent of ν. The only length scale independent of ν in this problem is d. Also deformations $\perp\hat{\mathbf{n}}$ involve all elastic constants: splay ($K_1 \sim K_3$), twist ($K_2 \sim K_3/3$), and bend (K_3) [7]. This result suggests $v_p \sim (2/d)K_{\text{eff}}/\gamma_1 \approx 32\ \mu$m/s with $K_{\text{eff}} \approx 2K_3/3$ using measured values for $K_3 = 1.26 \times 10^{-6}$ dyne and $\gamma_1 = 0.4$ dyne/cm^2/s [17]. $K_{\text{eff}} \sim (K_3 + K_2)/2$: twist and splay-bend deformations contribute equally in determining v_p.

In the same spirit, we estimate v_t by assuming a mismatch in curvature elasticity between adjacent rolls. This mismatch (Fig. 3c) arises because in half of the rolls, viscous torques work with $\mathbf{E}$ (A rolls), while in the other half, they compete with $\mathbf{E}$ (B rolls). For A rolls, n_x monotonically increases to its maximum at the roll (sample) center. For B rolls, while n_x increases through the boundary layers where $\mathbf{E}$ dominates, it decreases to a local minimum at the roll center where viscous torques dominate. We assume A rolls are locally much less energetic than B rolls.

To estimate v_t, we call β the maximum angle between $\hat{\mathbf{n}}$ and $\hat{\mathbf{x}}$ at the center of B rolls. Put $\beta \sim 0$ at its roll radius, $\lambda/4$, as well as in A rolls. Then after equating the elastic energy density difference between A and B rolls, $\Delta f \approx K_{\text{eff}}(4\beta/\lambda)^2$, to a viscous torque density, $4\beta\gamma_1 v_t/\lambda$, we get $v_t/v_p \approx 2\beta(d/\lambda)$. Consistent with observations, the smaller λ, the larger v_t (Fig. 4). An order of magnitude estimate for v_t is obtained by putting $\beta \approx 1$. Then, $v_t \sim 60\ \mu$m/s at $\nu = 10$ Hz where $\lambda/d \approx 1.1$ and increases to $v_t \sim 90\ \mu$m/s at 300 Hz where $\lambda/d \sim 0.7$. This rough estimate is surprisingly good at 10 Hz and less so at 300 Hz (Fig. 4). This suggests that β also increases

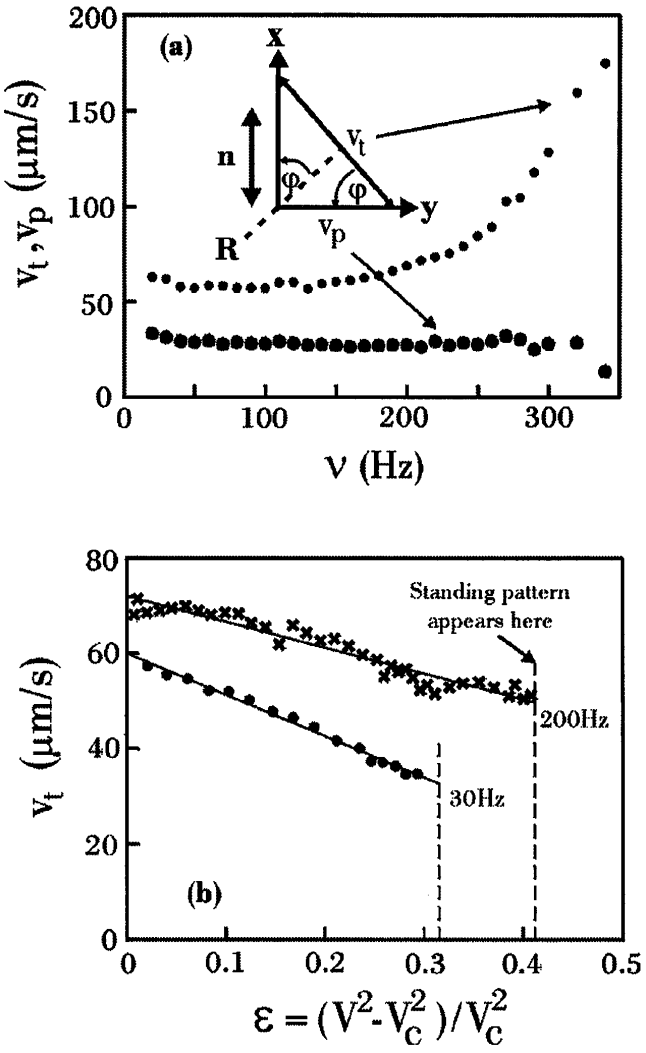

FIG. 4. $d = 13\ \mu$m. (a) $\mathbf{v_t} \perp \mathbf{R}$ and $\mathbf{v_p} \perp \hat{\mathbf{n}}$ vs ν. As ν increases ($\phi \to \pi/2$), v_p is approximately constant while v_t increases. (b) v_t as a function of the control parameter $\varepsilon = (V^2 - V_c^2)/V_c^2$ when $\nu = 200$ Hz ($\nu/\nu_c \sim 0.44$). At the standing stripe pattern onset, $v_t \sim 55\ \mu$m/s $\to 0$.

as λ decreases (ν bigger). A large enough β/λ ratio is needed to trigger the next instability which is not observed at any voltage when $\nu \lesssim 200$ Hz.

A subcritical bifurcation launches the second instability, a novel standing stripe pattern, when $0.40 < \nu/\nu_c < 0.78$ and $25 < V \equiv V_S < 50$ V (Figs. 1b, 3d, 4b). In this pattern, $\hat{\mathbf{n}}$ has a periodic component parallel to the roll axis ($n_y \neq 0$). This is an option as homeotropic boundary conditions allow $\hat{\mathbf{n}}$ complete xy freedom. Optical analysis shows maximum/minimum values for n_y associated with only one roll that we identify as the more energetic B rolls of the first pattern (Fig. 3d). The stripe pattern wavelength, λ_S, is thus $\lambda_S = 2\lambda \sim 24$ μm $\gtrsim d$ in Fig. 1b. With only weak elastic forces stabilizing it, the stationary stripe pattern occurs in a narrow voltage range.

When $V = V_Z \sim 1.1V_S$, viscous torques overcome the weak elastic ones stabilizing straight rolls leading to the Zvinger pattern. This pattern nucleates from a periodic line of roll disclinations at the stripe-Zvinger interface formed as torques of opposite sign spontaneously rotate rolls with maximum and minimum n_y in opposite directions to form roll arcs (Figs. 3d, 3e). With one Möbion every λ_S, $\lambda_Z = 2\lambda_S = 4\lambda \sim 40$ μm $\sim 2d$ (Figs. 1c, 3e). While now in the plane of shear, $\hat{\mathbf{n}} \perp \hat{\mathbf{R}}$, $\hat{\mathbf{n}}$ rotates 2π in λ_Z (Fig. 3e).

The uniform rotation of $\hat{\mathbf{n}}$ in a Zvinger is beautifully revealed when the field is turned off (Fig. 2). Möbions associated with Zvinger dislocations are also seen. The repulsive interactions observed between defects is additional evidence that they all have the same topological charge [7].

Figure 1d shows fully developed Zvingers close to the transition to Möbion turbulence. Here, the pattern wavelength is close to $2\lambda_Z$ at the onset setting the stage for the last bifurcation to spatiotemporal disorder and incoherent Möbion dynamics. When the field is turned off in the turbulent regime, many Möbions randomly scattered remain in the field of view (Fig. 2). The fastest way to recover the initial homeotropic orientation is to heat to the isotropic liquid then cool to the nematic phase. This is a last difference with the planar geometry where the uniform state is immediately recovered when the field is turned off in its turbulent regime.

In conclusion, we described a novel wavelength doubling cascade to Möbius disclination turbulence in a 3D anisotropic liquid. Roll patterns built on a nonlinear base state with, in addition, complete rotational freedom in planes $\perp \mathbf{E}$, contrast dramatically with those built on a uniform state [15]. The first instability is a Hopf bifurcation. Further from equilibrium, the oscillatory pattern subcritically bifurcates to a novel standing stripe pattern that in turn has a subcritical bifurcation to a curved roll pattern (Zvingers). Neither the stripe nor Zvinger pattern has been predicted or previously observed. Even the coarsening dynamics when the external field is removed depends on initial conditions. These observations provide important complementary information for theories based on small amplitude perturbations of a highly nonlinear base state that cannot predict Möbius disclination formation in anisotropic nonequilibrium systems.

We thank E. Chin and J. Goodby for 10E6. P. E. C. thanks the Alexander von Humboldt Foundation and the Universität Bayreuth for hospitality. C. F. thanks the ENS (Paris) for financial support.

[1] *Pattern Formation in Liquid Crystals*, edited by A. Buka and L. Kramer (Springer, New York, 1996).
[2] *Spatio-Temporal Patterns in Nonequilibrium Complex Systems*, edited by P. E. Cladis and P. Palffy-Muhoray (Addison-Wesley, Reading, MA, 1994).
[3] M. C. Cross and P. C. Hohenberg, Rev. Mod. Phys. **65**, 851 (1993).
[4] I. Chang, N. Turok, and B. Yurke, Phys. Rev. Lett. **66**, 2472 (1991).
[5] V. M. Ruutu, V. B. Eltsov, A. J. Gill, T. W. Kibble, M. Krusius, Y. G. Makhlin, B. Placais, G. E. Volovik, and W. Xu, Nature (London) **382**, 334 (1996); C. Bäuerle, Y. M. Bunkov, S. N. Fisher, H. Godfrin, and G. R. Pickett, Nature (London) **382**, 332 (1996).
[6] See, for example, W. H. Zurek, Nature (London) **317**, 505 (1985).
[7] P. G. de Gennes and J. Prost, *The Physics of Liquid Crystals* (Clarendon Press, Oxford, 1993), 2nd ed.
[8] F. C. Frank, Discuss. Faraday Soc. **25**, 19 (1958).
[9] P. E. Cladis and M. Kléman, J. Phys. (Paris) **33**, 591 (1972).
[10] S. Kai and W. Zimmermann, Prog. Theor. Phys. Suppl. **99**, 458 (1989); L. Kramer and W. Pesch, Annu. Rev. Fluid Mech. **27**, 515 (1995).
[11] As nematics have no intrinsic length scale, V_F and V_c are independent of sample thickness, d.
[12] A. Hertrich, W. Decker, W. Pesch, and L. Kramer, J. Phys. (France) II **2**, 1915 (1992); A. Hertrich (private communication).
[13] H. Richter, N. Kloepper, A. Hertrich, and A. Buka, Europhys. Lett. **30**, 37 (1995).
[14] S. Kai, K. Hayashi, and Y. Hidaka, J. Phys. Chem. **100**, 19 007 (1996).
[15] H. R. Brand, C. Fradin, P. L. Finn, W. Pesch, and P. E. Cladis, Phys. Lett. A **235**, 508 (1997).
[16] P. Keller, P. E. Cladis, P. L. Finn, and H. R. Brand, J. Phys. (Paris) **46**, 2203 (1985).
[17] C. Fradin *et al.* (unpublished).
[18] 10E6: 4'-hexyloxyphenyl 4-decyloxybenzoate.